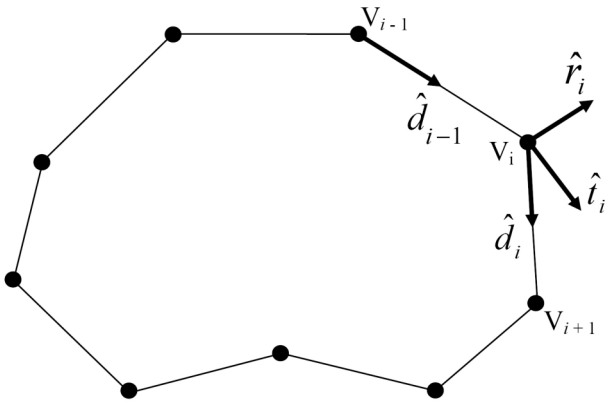

Figure 1. Configuration of the DDC. See the text for symbols. Reprinted with permission from the AAPM.

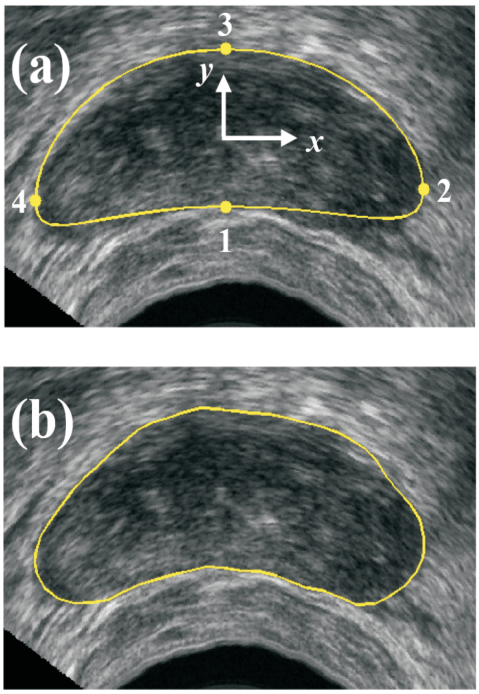

Figure 2. Initialization and deformation stages of the prostate segmentation algorithm. (a) Initial outline showing the four user-selected points, labeled (1)–(4) along with the local $x - y$ coordinate system defined from these points. (b) Final outline obtained after deforming the DDC. Reprinted with permission from the AAPM.

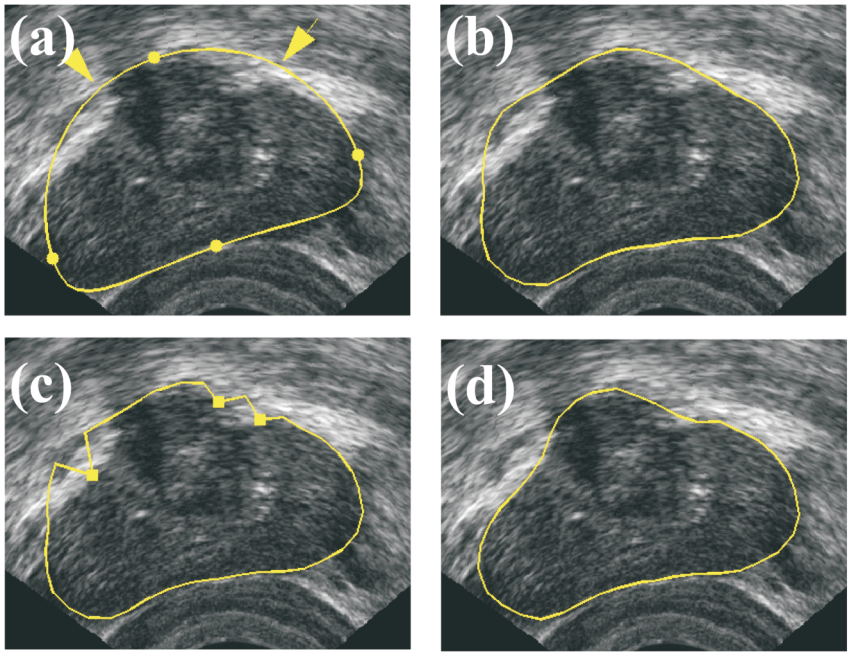

Figure 3. Illustration of interactive editing. (a) Initial DDC showing the four user-selected points. The portions of the DDC that do not follow the prostate boundary very well are indicated by arrows. (b) After first deformation. (c) Three vertices (squares) are dragged to new positions and clamped, and the DDC is deformed again. (d) After re-deformation. Reprinted with permission from the AAPM.

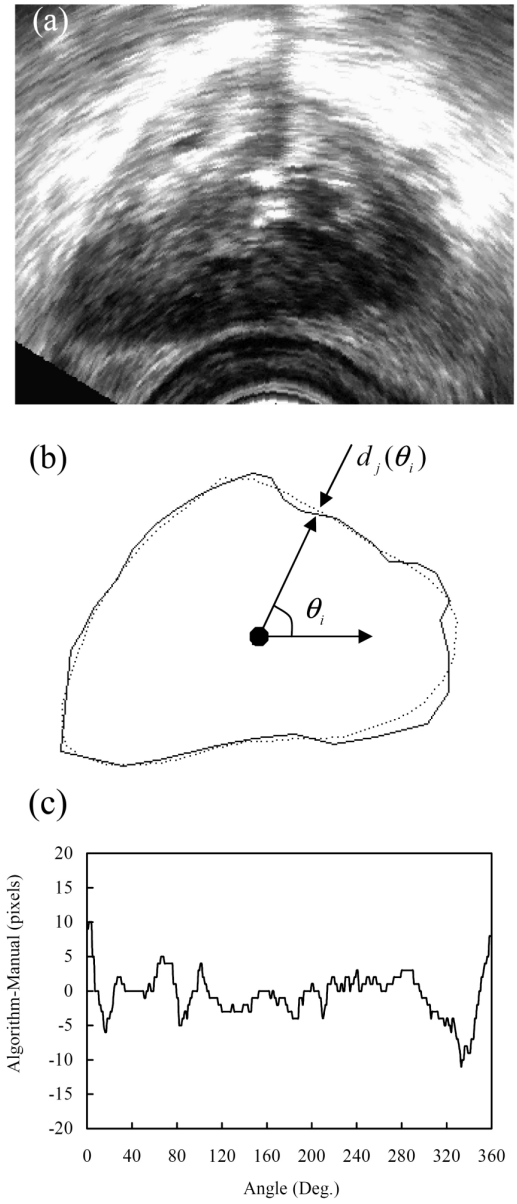

Figure 4. Local signed distance, $d_j(\theta_i)$, between two boundaries. (a) Sample prostate image. (b) Manual- (solid) and algorithm- (dotted) outlined boundaries. (c) $d_j(\theta_i)$ calculated for boundaries in (b). Reprinted with permission from the AAPM.

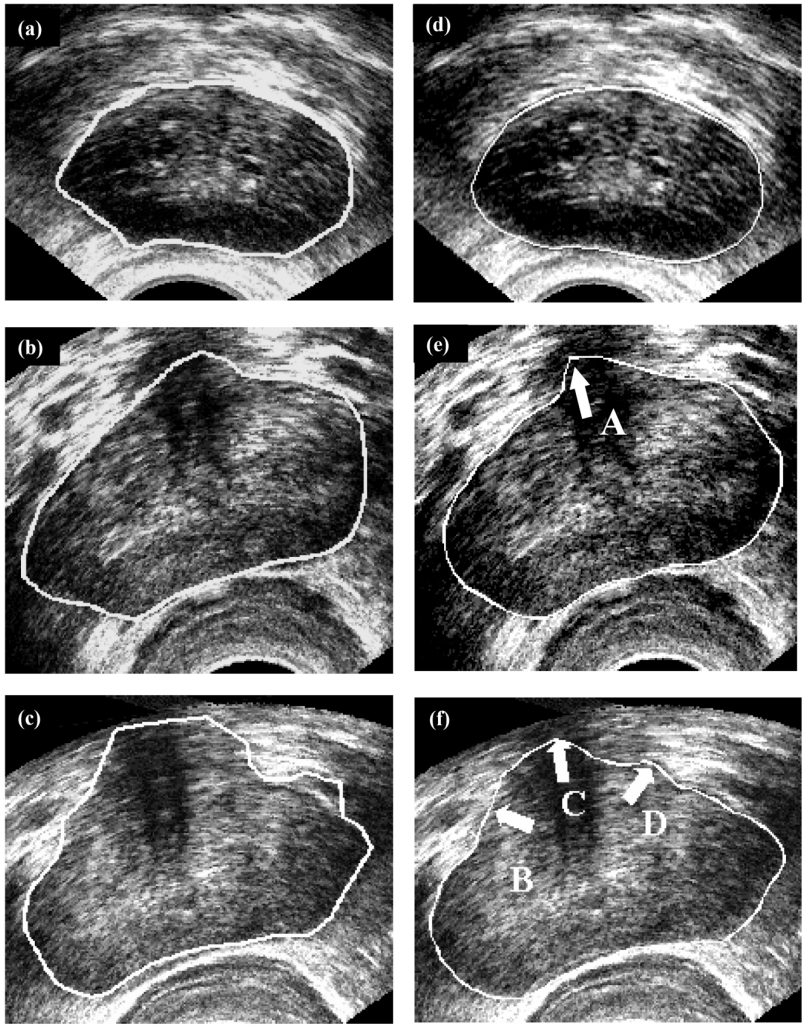

Figure 5. Comparison of manual- and algorithm-outlined boundaries for three categories: (a,d) easy; (b,e) moderate; (c,f) difficult. Reprinted with permission from the AAPM.

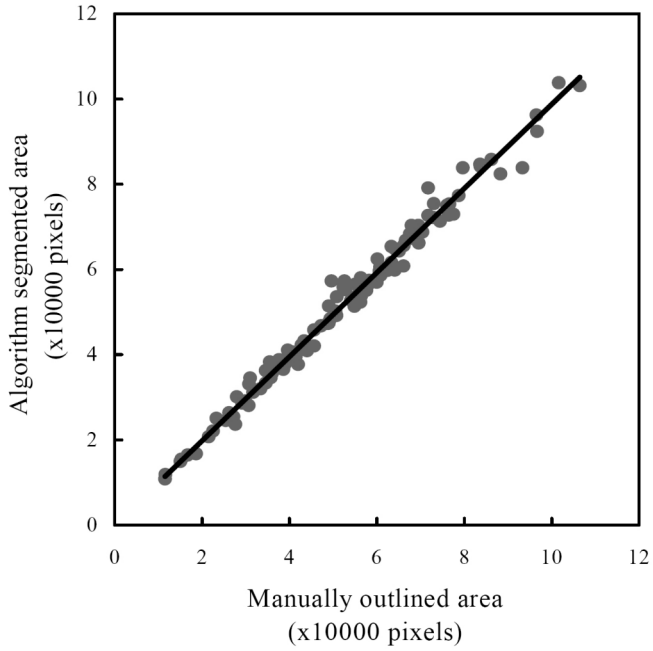

Figure 6. Area enclosed by algorithm-segmented outline versus corresponding area enclosed by manually outlined area. Reprinted with permission from the AAPM.

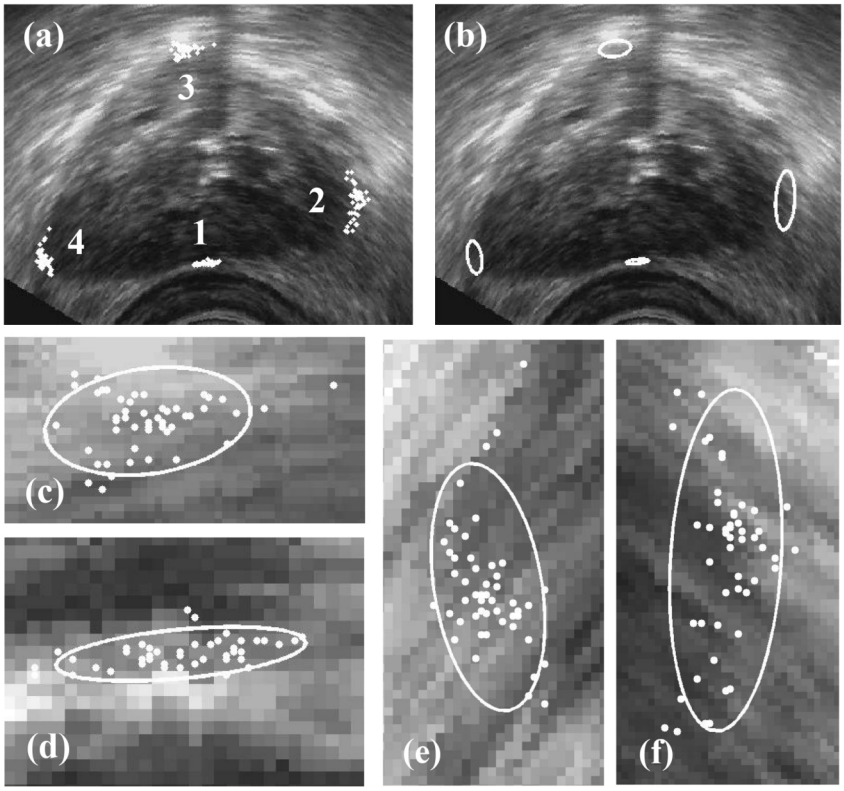

Figure 7. Construction of population distributions $p_{c,i}^{\mathrm{pop}}(x, y)$. Shown are (a) all 50 selections per control point made by five users on 10 different occasions; (b) ellipses enclosing 95% of selections along the principal axes of distributions $p_{c,i}^{\mathrm{pop}}(x, y)$ that are fitted to samples in (b); closeup views of selections for control points (c) 3, (d) 1, (e) 4, and (f) 2 along with ellipses enclosing the corresponding $p_{c,i}^{\mathrm{pop}}(x, y)$ are also shown. Reprinted with permission from the AAPM.

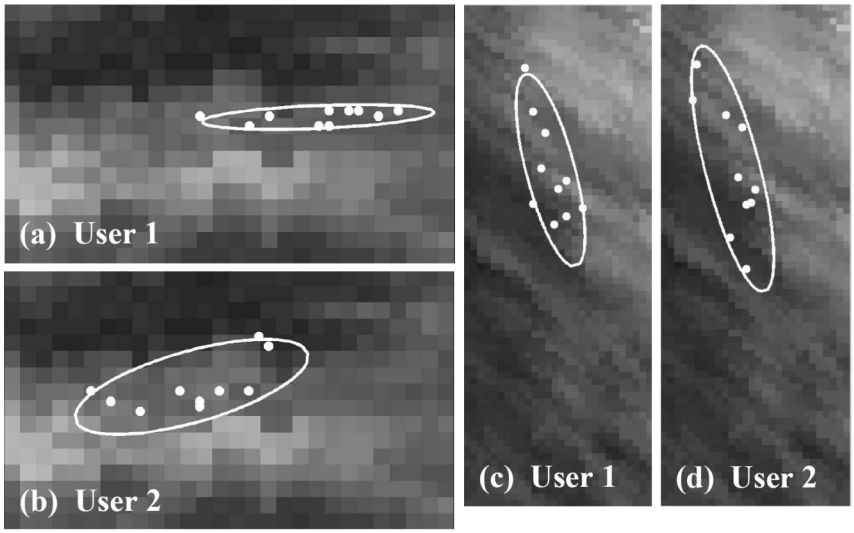

Figure 8. Sample individual selections and distributions $p^{\mathrm{ind}}_{u,c,i}(x,y)$ for 2 control points in Figure 1a. (a) Control point 1, user 1; (b) control point 1, user 2; (3) control point 2, user 1; (4) control point 2, user 2. Each user made 10 selections of the control point for the same image as in Figure 1a. The ellipses enclose 95% of samples along the principal axes of $p^{\mathrm{ind}}_{u,c,i}(x,y)$. Reprinted with permission from the AAPM.

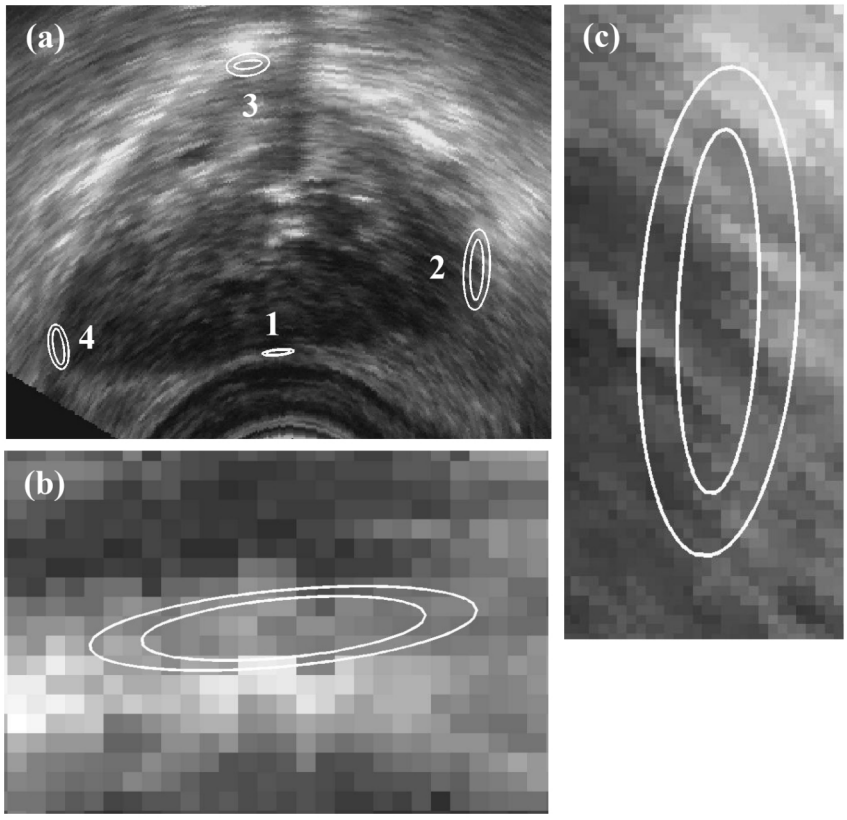

Figure 9. (a) Population, $p_{c,i}^{\mathrm{pop}}(x,y)$, and virtual operator, $p_{c,i}^{\mathrm{VO}}(x,y)$, distributions for the image shown in Figure 1. The larger ellipses represent the spatial extent of $p_{c,i}^{\mathrm{pop}}(x,y)$, whereas the smaller ones represent $p_{c,i}^{\mathrm{VO}}(x,y)$. (b) Closeup of control point 1. (c) Closeup view of control point 2. Reprinted with permission from the AAPM.

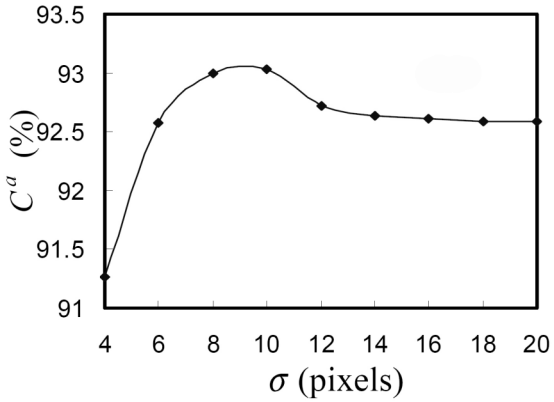

Figure 10. C_i^a computed for values of σ from 4 pixels to 20 pixels for the image in Figure 7a: $w^{\mathrm{int}} = 0.25$ and $w^{\mathrm{img}} = 0.75$. Reprinted with permission from the AAPM.

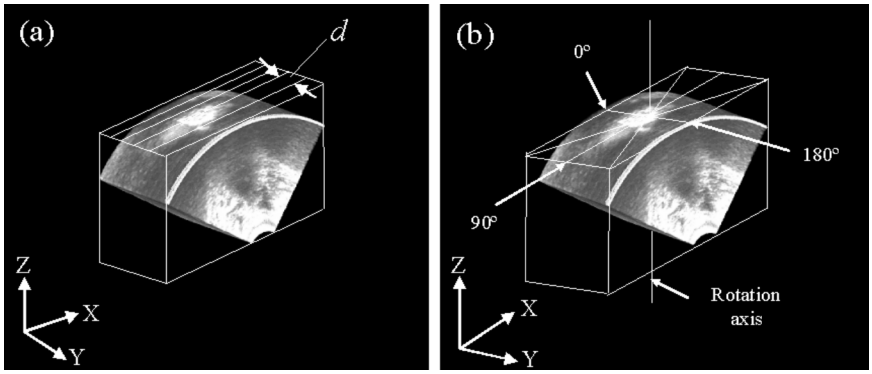

Figure 11. Two different re-slicing methods: (a) parallel re-slicing along the y-axis with spatial spacing (d); (2) rotationally re-slicing along the z-axis with uniform angular spacing. Reprinted with permission from the AAPM.

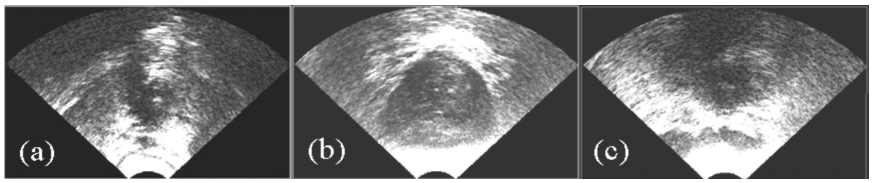

Figure 12. Three different slices in parallel re-slicing: (a) at the front end of the prostate; (b) in the middle of the prostate; (b) at the back end of the prostate. Reprinted with permission from the AAPM.

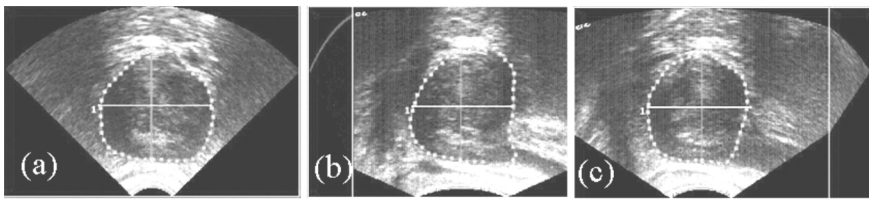

Figure 13. Three different slices in rotationally re-slicing of the same prostate: (a) slice at $0°$; (b) slice at $45°$; (b) slice at $90°$. The dotted contour is the prostate boundary outlined by the operator. Reprinted with permission from the AAPM.

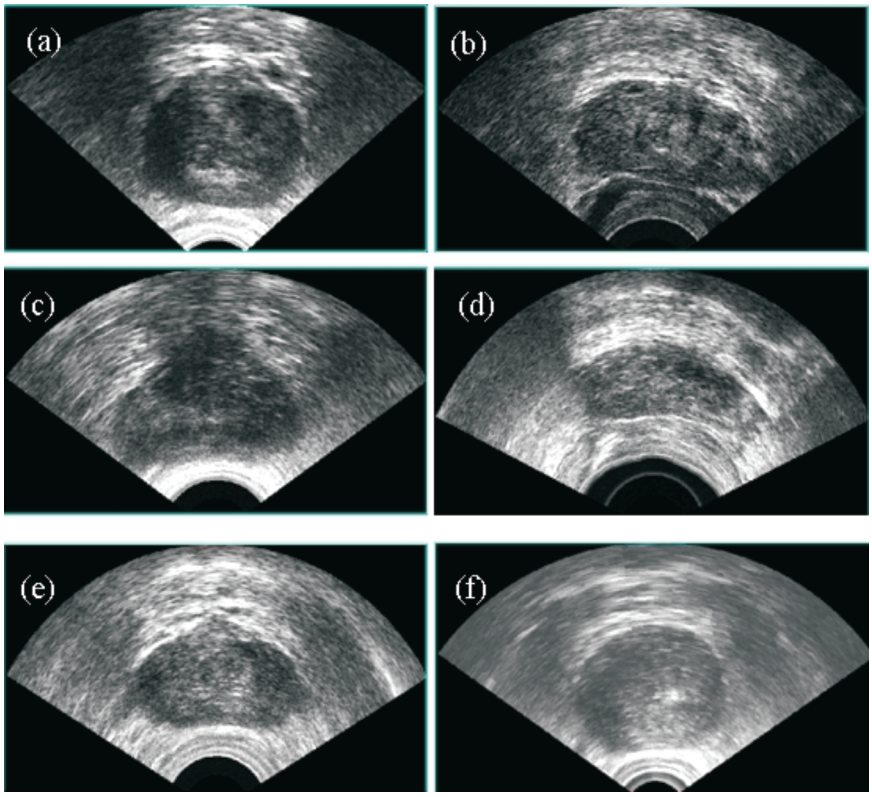

Figure 14. Initial segmentation slices of six different 3D TRUS prostate images obtained from different patients. (a) This 3D TRUS image was used to determine the classification criterion for selection of the vertex on the clockwise or anti-clockwise contours. (b–f) These 3D TRUS images were used to evaluate the segmentation algorithms. Reprinted with permission from the AAPM.

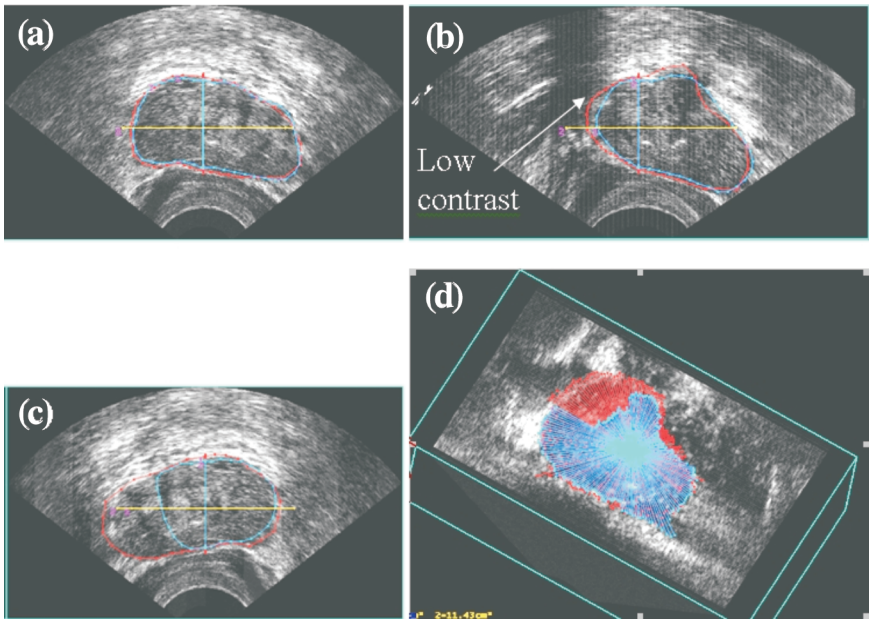

Figure 15. Illustration of error accumulation in the slice-based 3D prostate segmentation method. The 3D prostate was rotationally re-sliced into 90 slices, and their 45th, 48th, and 56th slices are shown in (a)–(c). In each slice the manual (GRAY) and automatically (WHITE) segmented contours are presented. In the center of these slices, the vertical line is the rotational axis while the horizontal line represents the coronal cross-sectional plane. (d) Coronal cross-sectional view of the manually and algorithm-segmented prostate contours.

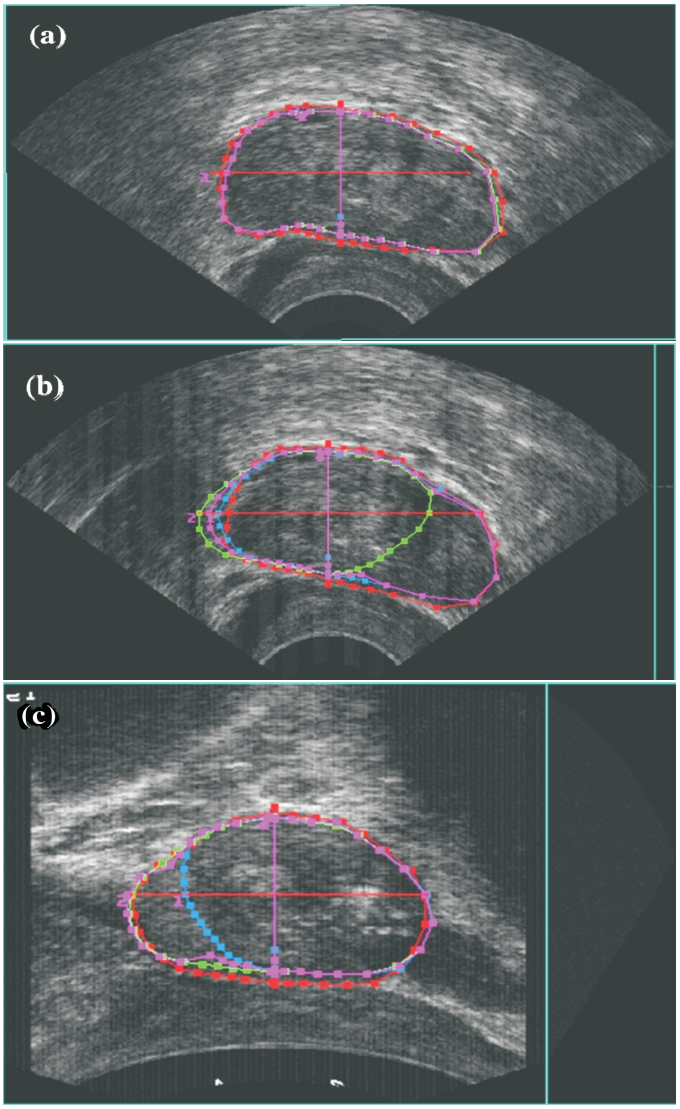

Figure 16. Optimal combination of clockwise and anti-clockwise propagated prostate contours of Figure 5b. The vertical line is the rotational axis of re-slicing and the horizontal line is the cross-sectional plane. Four contours are shown: manual (red), clockwise propagation (green), anti-clockwise propagation (blue), and optimal contour (purple). (a) 0th slice, i.e., the initial slice; (b) 17th slice, the blue contour is optimal; (c) 59th slice, green contour is optimal.

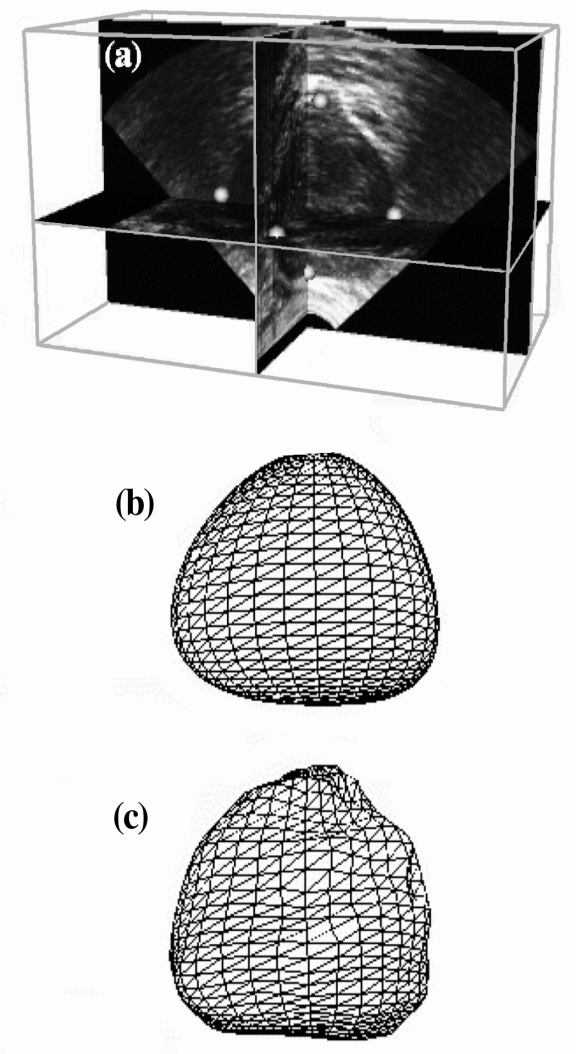

Figure 17. Illustration of steps in the operation of the 3D deformable model based segmentation algorithm: (a) 3D TRUS image with 5 of the 6 user-selected control points shown as white spheres; (b) initial mesh; (c) deformed mesh. Reprinted with permission from the AAPM.

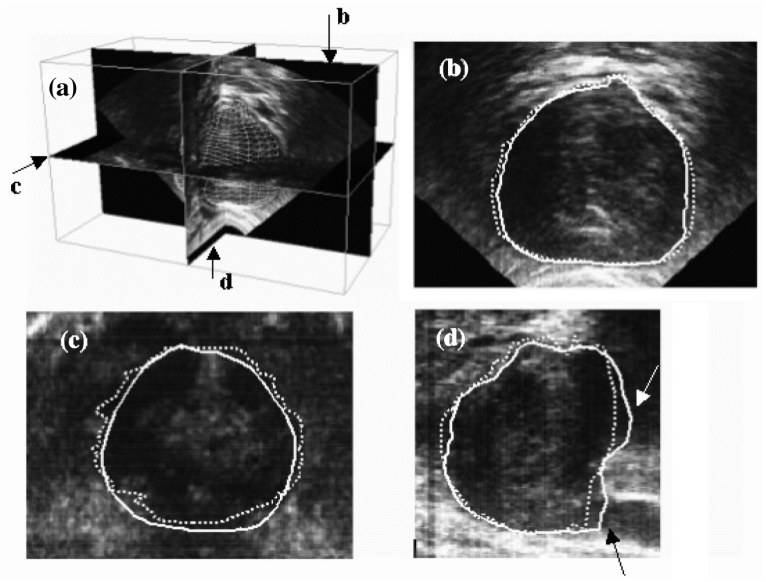

Figure 18. Cross-sections through the image in Figure 17 along with the algorithm segmentation (solid line) and manual segmentation (dotted line). (a) 3D TRUS image of the prostate with transverse, coronal, and sagittal cutting planes indicated by (b–d), respectively, to show 2D cross-sectional images. (b) Transverse cross-section of the image and the boundaries corresponding to the plane shown in (a). (c) Coronal cross-section of the image and the boundaries. (d) Sagital cross-section of the image and boundaries. Reprinted with permission from the AAPM.

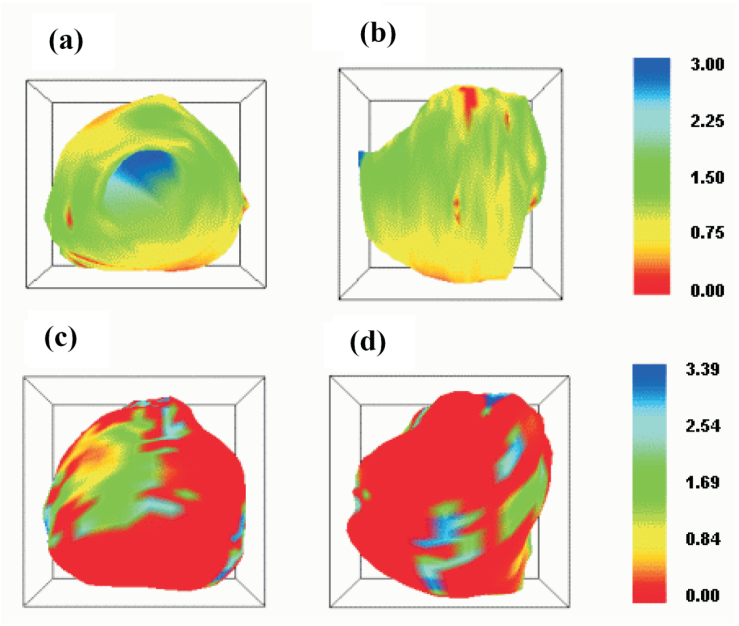

Figure 19. Local standard deviation maps: (c,d) Local standard deviation mapped on the average manually segmented boundary. (e,f) Local standard deviation mapped on the average algorithm-segmented boundary. Red regions indicate zero standard deviation and blue regions represent maximum standard deviation, which was 3.0 for manual and 3.4 mm for algorithm segmentation. The left-hand column is a view of the prostate perpendicular to the transverse plane in the direction from the base to the apex, whereas the right-hand column is a view perpendicular to the sagital plane in the direction from the patient's right to left. Reprinted with permission from the AAPM.